Extraction of Pig Farms From GaoFen Satellite Images Based on Deep Learning

Jielin Guan, Le Li, Zurui Ao, Kefei Zhao, Yaozhong Pan, and Weifeng Ma

***Abstract*—Accurate information on the spatial distribution and area of pig farms is essential for pig breeding monitoring, pork production estimation, and environmental governance of pig breeding. Governmental regulatory departments mostly rely on field surveys to obtain pig farm information, and there are few studies that focus on the extraction of pig farm information using remote sensing data. As the buildings on pig farms are small-scale and have scattered distributions, pig farm identification using high-resolution data and deep learning algorithms is worth exploring. In this article, a method of identifying pig farms with a deep learning algorithm and multiple sources of GaoFen (GF) image data was proposed. The experiments were conducted with different combinations of multiple sources of GaoFen satellite images (GF-2, GF-5, and GF-7) to determine the suitability of these images for pig farm extraction. The results illustrated that the average overall accuracy of the pig farm identification was above 80% using all of the different combinations of GaoFen sourced images. The spatial detail information provided by the GF-2 satellite improved the pig farm identification accuracy more than did the spectral detail information provided by the hyperspectral data from the GF-5 satellite and the digital surface model from the GF-7 satellite. The deep learning algorithm performed well in identifying pig farms with a greater number of patches and a higher aggregation index, and had lower accuracy in extracting pig farms distribution with a high edge density and patch density.**

***Index Terms*—Building extraction, deep learning, pig farms, satellite images.**

I. Introduction

CHINA is the world's largest pork producer and consumer [1]. The pig industry is an important part of the modern agricultural system and leads other industries in animal husbandry in China [2]. With the development of modern animal husbandry, pig breeding has changed from a small-scale (individual households) to an intensive and large-scale (large farms) industry [3], [4]. These changes have included the movement away from free-range breeding and the transfer of pigs from pens to farms [5], [6]. Large-scale breeding has improved the quality of the industrial supply, but it has introduced monitoring challenges. Accurate information on the spatial distribution and area of pig farms is essential for pig breeding monitoring, pork production estimation, and environmental governance of pig breeding [7], [8]. These data provide support for governmental decision making for pig breeding management from the perspective of spatial information.

In the past, governmental regulatory departments mostly relied on field surveys to obtain pig farm information [9]. Although the pig breeding industry is moving toward aggregation, the spatial distribution of pig farms is still scattered [10]. Thus, field surveys on pig farms are time consuming and labor intensive. After African swine fever and other epidemics, on-site investigations have been increasingly restricted by farm owners due to breeding safety considerations, making pig breeding investigations increasingly difficult. With the development of satellite remote sensing technology, high-resolution remote sensing images have been widely used to provide large-scale and rapid Earth observations [11]. High-resolution remote sensing images are widely used in the extraction of different types of land uses [12]. Pig farms include functional buildings where humans raise piglets and grow them into adult pigs [13]. In the past two decades, the rapid development of computer technology and satellite remote sensing technology has made tremendous progress in building extraction-related research [14].

Traditional building extraction methods mainly rely on the artificial creation of building features, including spectral, shape, and texture features [15], [16], [17], [18]. There are some spectral indices specifically proposed for architectural features, such as the normalized building index (NDBI) [19], index based built-up index (IBI) [20], and morphological building index (MBI) [21]. Then, with the help of machine learning classifiers, automatic identification of buildings can be achieved. The main machine learning classifiers used are decision trees [22], random forests [23], and support vector machines, [24], [25] and with the continuous improvement of classifiers, the efficiency and accuracy of building extraction have been greatly improved. However, machine learning methods still require manual participation in feature design and cannot adaptively extract the most relevant features for classification tasks. Artificially designed features rely on expert knowledge, and there are certain defects in their robustness and generalization ability. When the imaging conditions and shooting angles of the images change, these

Manuscript received 19 July 2023; revised 14 September 2023; accepted 6 October 2023. Date of publication 10 October 2023; date of current version 24 October 2023. This work was supported in part by the Major Project of High Resolution Earth Observation System (Civil Part) under Grant 20-Y30F10-9001-20/22, and in part by the Natural Science Foundation of Guangdong Province of China under Grant 2023A1515010897 and Grant 2020A1515110341. *(Corresponding author: Le Li.)*

Jielin Guan, Le Li, and Kefei Zhao are with the School of Management, Guangdong University of Technology, Guangzhou 510520, China (e-mail: 2112008076@mail2.gdut.edu.cn; lilegeo@gdut.edu.cn; zhaokf@gdut.edu.cn).

Zurui Ao is with the Beidou Research Institute, Faculty of Engineering, South China Normal University, Foshan 528000, China (e-mail: aozurui1990@gmail.com).

Yaozhong Pan is with the State Key Laboratory of Remote Sensing Science, Beijing Normal University, Beijing 100875, China (e-mail: pyz@bnu.edu.cn).

Weifeng Ma is with the Piesat Information Technology Company Ltd., Beijing 100195, China (e-mail: weifeng.ma@foxmail.com).

Digital Object Identifier 10.1109/JSTARS.2023.3323486

© 2023 The Authors. This work is licensed under a Creative Commons Attribution-NonCommercial-NoDerivatives 4.0 License. For more information, see https://creativecommons.org/licenses/by-nc-nd/4.0/

features become unreliable and accurate good classification results cannot be obtained.

Deep learning is making great progress in the computer vision field in recent years and is widely used in the classification, recognition and retrieval of remote sensing images [26], [27], [28]. The advantage of deep learning is that, on the one hand, it can automatically learn different levels of features by just training the dataset, without having to manually define the features for the task [29]. On the other hand, deep learning has better generalization ability and can satisfy other tasks by fine tuning the original neural network without redesigning the features for different datasets, and it has better noise immunity [30], [31]. Deep learning is more accurate in image recognition than human interpretation, which means that automatically identifying pig farms from remotely sensed images can achieve reasonable results based on deep learning [32]. Despite previous researchers have utilized deep learning in land use classification and surface object detection, there is still relatively limited researches specifically focused on deep learning methods for the identification of functional buildings, such as pig farms [33], [34], [35]. Unlike typical functional buildings, the pig farming facilities are usually arranged in a linear and array-like distribution in order to accommodate pig breeding in large scale, and they are always built with simpler roofing materials than residential buildings [36], [37]. The spectral differences of these distinct morphology and material features in remote sensing imagery make it worthwhile to explore deep learning networks and their applicability for pig farm identification.

Many deep learning networks have been developed, among which the convolutional neural network (CNN) is one of the most widely used network in the field of remote sensing. CNNs have strong image processing capabilities and are superior in extracting high-level and distinguishing features. For building extraction, there are many networks designed specifically based on CNN structures, such as fully convolutional networks (FCNs) [38], deep CNNs (DCNNs) [39], deep deconvolutional neural networks (DeCNNs) [40], and object-oriented CNNs (OCNNs) [41]. All these methods validate the effectiveness of the CNN in building extraction. However, CNNs mainly utilize high-level feature maps for pixel classification and pay less attention to low-level features containing rich detail, which is detrimental to the extraction of small buildings. To solve this problem, semantic segmentation methods based on excellent networks have been promoted, such as U-Net, ENet, and SegNet [42], [43], [44]. These networks retain both rich spatial information and fine detail and are more suitable for small building targets in remote sensing images with complex backgrounds. Among deep learning networks, U-Net has a simple network structure and is highly resistant to interference [45], [46], [47]. As a representative of lightweight deep learning networks, it has been applied in objects identification with small training set and has a good detection ability in short amount of time [48], [49]. However, its performance in pig farm extraction has rarely been investigated.

In the past decade, China has independently launched and operated various GaoFen satellites, such as the GF-1/GF-2 multispectral satellites, GF-3 radar satellite, GF-5 hyperspectral satellite, and GF-7 satellite, to fulfil ground monitoring needs. Among these, the GF-2 satellite provides high-resolution images, the GF-5 satellite offers high-spectral resolution images, and the GF-7 satellite provides stereo image pairs that can be used to extract DSM. The combined use of these GaoFen data sources creates new opportunities for farm extraction, and it is imperative to study their effectiveness in this context. Thus, in this study, the U-Net model is used to extract pig farms and obtain a spatial distribution map of pig farms on a regional scale. Based on this, the main objectives of this study are as follows:

1) validate the effectiveness of deep learning for pig farm extraction;
2) compare the accuracy of Gaofen multispectral images, hyperspectral images, and the DSM combination strategy on pig farm extraction;
3) compare the identification accuracy of pig farms with different morphological characteristics.

II. Study Area and Materials

A. Study Area Description

We selected four counties in Shandong as study area. Shandong is on the North China Plain, with a flat terrain and a temperate monsoon climate. It is the fourth largest pig breeding province and an important province for pig transfer in China, bearing the heavy burden of pork supply in northern China [50]. The number of registered live pigs in Shandong is more than 28 million, and more than 50 million pigs are slaughtered annually, with pork production reaching more than 4 million tons, accounting for 7% of the national pork production and 4% of the world's pork production each year.[1] Studying the spatial distribution of pig farms in Shandong is of strategic importance to promote stable and healthy development of the pig industry in China. In recent years, the industrial organization of pig farming in Shandong has been optimized, and the pig industry has been strategically adjusted. At present, Shandong focuses on the development of large-scale pig farming, and it contains many large-scale pig farms. In addition, Shandong is in northern China, which is less affected by clouds and rain throughout the year, thus there is sufficient remote sensing earth observation data from this region. In this article, the pig breeding scale in Shandong Province was divided into four classes according to the 2020 pig breeding capacity of each county in the province, from which four counties were selected as the study area. These four counties were Jiyang County (116°52′-117°27′E, 36°41′-37°15′N), with an annual pig breeding capacity $<$200000; Zouping County (117°18′-117°57′E, 36°41′-37°08′N), with an annual pig breeding capacity $<$20 0000 and $>$500 000; Laixi County (120°12′-120°40′E, 36°34′-37°09′N), with an annual pig breeding capacity $<$1 000 000 and $>$500 000; and Cao County (115°08′-115°53′E, 34°33′-35°03′N), with an annual pig breeding capacity $>$1 000 000.

[1] [Online]. Available: http://www.stats.gov.cn/sj/ndsj/

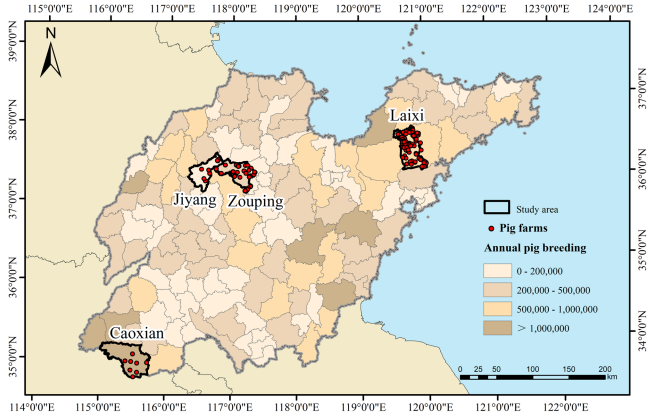

Fig. 1. Distribution of pig farms in the study area.

B. Field Survey Data

A field survey was carried out from December 2021 to May 2022 to collect geographical location information for pig farm identification. A total of 134 pig farms were included in the field survey. Among them, 39 are medium-sized farms and 95 are large farms. The medium-sized pig farms refers to the pig farms with annual pig rearing capacity greater than 500 and less than 5000, while the large-sized pig farms refers to the pig farms with annual pig rearing capacity greater than 5000. Here, annual rearing capacity equals the sum of year-end pig stock and annual pig slaughtering capacity. Among all the collected pig farms, there were 80 pig farms in Laixi, 37 pig farms in Zouping, 9 pig farms in Jiyang, and 8 pig farms in Caoxian (see Fig. 1).

C. Remote Sensing Data Sources and Preprocessing

The GaoFen family is a series of Chinese remote sensing satellites developed by the China High-definition Earth Observation System (CHEOS) for civilian purposes. Three GaoFen satellites, including GF-2 (with multispectral images), GF-5 (with hyperspectral images), and GF-7 (with stereo images), were selected (see Table I). The GF-2 satellite can provide observation products with a spatial resolution of better than 1 m, which is configured with four multispectral 3.2-m bands and one panchromatic 0.8-m band. It has an efficient revisit frequency of five days [51]. The GF-5 satellite carries six payloads: two hyperspectral/multispectral payloads for terrestrial Earth observation and four atmospheric observation payloads [52]. The product generated from the Advanced Hyperspectral Imager (AHSI) has a 330-channel imaging spectrometer with a spectral range of 0.4–2.5 μm, covering visible to shortwave infrared bands. The spatial resolution of its products is 30 m, and the swath width is 60 km [53]. The revisit frequency is 51 days. GF-7 is a high-resolution stereo mapping satellite equipped with double-line cameras (DLCs) that are capable of capturing backwards images of 0.65-m resolutions and forwards images of 0.8-m resolutions, which can be processed to provide elevation information. The revisit frequency of stereo mapping observations is 60 days. The level 1A GF-2 and GF-7 products and the level 1 GF-5 product with cloud coverage of less than 10% were downloaded from the China Resource Satellite Application Center (http://www.cresda.com/CN/).

The available data included 37 scenes from GF-2, 7 scenes from GF-5, and 25 scenes from GF-7 (see Table II). The GF satellite data volume covering the pig farms in the study area is shown

TABLE I
SPECIFICATIONS FOR GF-2, GF-5, AND GF-7

	GF-2	GF-5	GF-7
Launch time	19 August 2014	9 May 2018	3 November 2019
Revisit cycle (days)	5	51	60
Swath width (km)	45	60	20
Sensors	pms	ahsi*; vims; gmi; aius; emi; dpc	dlc*; la; fc
Spatial resolution (m)	pan: 0.8 mux: 3.2	30	pan-fwd: 0.8 pan-bwd: 0.65 mux: 2.6
Number of Bands	4	vnir: 150 swir: 180	4
Wavelength (nm)	pan: 450–900 blue: 450–520 green: 520–590 red: 630–690 infrared: 770–890	400–2500	pan: 450–900 blue: 450–520 green: 520–590 red: 630–690 infrared: 770–890

(pms = panchromatic and multispectral, pan = panchromatic bands, mux = multispectral bands, fwd = forwards, bwd = backwards, ahsi = advanced hyperspectral imager, vims = visual and infrared multispectral sensor, gmi = greenhouse gases monitoring instrument, aius = atmospheric infrared ultraspectral, emi = environment monitoring instrument, dpc = directional polarization camera, dlc = double-line camera, la = laser altimeter, Fc = footprint camera).

TABLE II
DETAILS OF THE EMPLOYED GF-2, GF-5, AND GF-7 SATELLITE DATA

Data resource	Data type	Acquisition dates (Year/Month)	Number of images
GF-2	Multispectral image	2019/3–2021/10	37
GF-5	Hyperspectral image	2019/5–2020/3	7
GF-7	Stereo images	2020/3–2021/12	25

Fig. 2. Datasets used in this study. (a) Coverage of multiple GaoFen satellite data source. (b) Example of pig farm.

in Fig. 2. Ortho-rectification and fusion with Gram Schmidt (GS) fusion were implemented on GF-2 MUX images and GF-2 PAN images. The GF-2 products were resampled to 0.8 m. Redundant bands, including noisy bands due to atmospheric water absorption (band: 192–203; 246–267; and 314–316), overlapping bands between visible and near-infrared (VNIR) and shortwave infrared (SWIR) bands (band: 151–154) and bands with low signal-to-noise ratios (bands: 325–330), were removed from the GF-5 AHSI. Furthermore, the remaining 284 bands were preprocessed with radiometric calibration and atmospheric correction in the Fast Line-of-Sight Atmospheric Analysis of Spectral Hypercubes model (FLAASH), and dimensionality reduction was performed using the principal component analysis (PCA) method. A digital surface model (DSM) with a resolution of 0.8 m was extracted from GF-7 forwards and backwards images. Finally, both the hyperspectral image from GF-5 and the DSM from GF-7 were registered with GF-2 as a reference.

III. Materials and Methods

A. Sample Selection

In this study, the ground-truthed binary maps of the pig farms were manually labeled on GF-2, GF-5, and GF-7 by visual interpretation to create deep learning samples. The labels on the samples included the area of the pig farms and their ancillary facilities. If parts of the pig farms were covered by branches and cloud shadows, the boundaries of those pig farms were determined by the visible area on orthophoto images. Since there were only 62 pig farms that could be simultaneously covered by GF-2, GF-5, and GF-7, to ensure the comparability of the results of different subsequent experimental schemes, only those 62 pig farms were used to create the samples. All the samples were clipped into 224∗224 pixel images, with a moving window step of 112 pixels. The samples were randomly divided into training and test sets at a 9:1 ratio for tenfold cross validation. Flipping and rotation were used to expand the training sample volume. Each training sample was rotated by 90°, 180°, and 270° and flipped vertically and horizontally. Finally, 13 122 training samples in total were generated from the three GaoFen satellites with 224∗224 pixel sizes.

TABLE III
Experimental Design With GF-2, GF-5, and GF-7

Experimental group	GF-2	GF-5	GF-7
A	○		
B		○	
C	○	○	
D	○		○

*○ donates the data used.

B. Experimental Design and Operational Process

To verify the applicability of multiple sources of GaoFen satellite images for pig farm extraction, we designed our experiments with different combinations of GaoFen satellite image sources, including three different satellites, GF-2, GF-5, and GF-7. The four groups of experiments are shown in Table III, with multispectral data from GF-2 in group A, hyperspectral data from GF-5 in group B, a combination of multispectral data from GF-2 and hyperspectral data from GF-5 in group C, and a combination of multispectral data from GF-2 and stereo images from GF-7 in group D. To exclude the effect of the spatial resolution on identification accuracy, the GF-5 hyperspectral data were fused with the GF-2 panchromatic images during data preprocessing, and the fused GF-5 spatial resolution was 0.8 m.

C. Pig Farm Extraction Based on the U-Net Model

The U-Net deep learning network was trained on the pig farm features in the GaoFen image series, and the trained U-Net was implemented to identify the spatial distribution of pig farms. The trained U-Net was designed to include an encoder that extracted semantic information and a decoder that was symmetrical to the encoder. They were implemented in the downsampling and upsampling processes, respectively. The detailed architecture of U-Net is shown in Fig. 3. The structure of the encoder is typical of a CNN, composed of stacked convolutional and max pooling layers designed to extract maps of the features, such as the boundaries, positions, colors, and shapes, from the pig farm images. By comparison, the decoder upsamples and deconvolutes the feature maps several times, which can help restore the feature images to their original size. In the upsampling path in the decoder, the decoder fuses with the corresponding feature map in the encoder with skip connections, providing much of the low-level information for upsampling or deconvolution and recovering the details of the image.

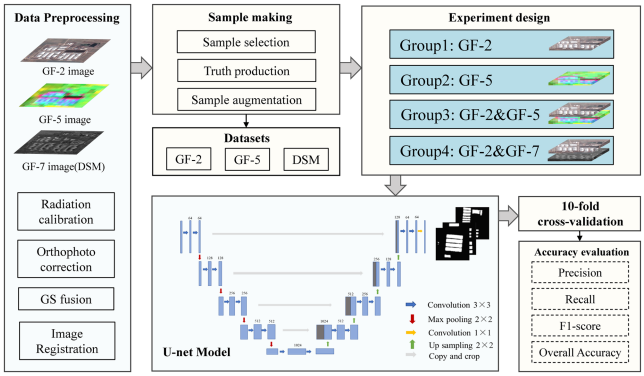

Fig. 3. Workflow for pig farm extraction.

After several training and testing validations, the key initial parameters were set with an initial learning rate of 5 × 10-4, a learning rate decay rate of 0.8, a step size of 20 and a gradient update weight momentum of 0.9. To avoid overfitting, the weight decay was set to 1 × 10-6. The model optimizer algorithm was set to Adam. The epoch was set to 200. The same model structure and the same parameters were used in the four groups of experiments.

D. Deep Learning Model Evaluation

Four indicators, including precision, recall, overall accuracy (OA), and the F1-score, were used to evaluate the extraction results for each experimental group. Precision was defined as the ratio of the correctly extracted pig farms in all the positive pig farm samples, while recall was defined as the ratio of the correctly extracted pig farms in all the positive pig farm samples in the ground surveys. The OA indicated the accuracy of the extraction results being consistent with the ground surveys. The F1-score was a harmonic average of the two evaluation methods and could be used to comprehensively evaluate the commission and omission errors. These indicators were defined as follows:

$$\text{Precision} = \text{TP}/(\text{TP}+\text{FP}) \quad (1)$$

$$\text{Recall} = \text{TP}/(\text{TP}+\text{FN}) \quad (2)$$

$$\text{OA} = (\text{TP}+\text{TN})/(\text{TP}+\text{TN}+\text{FP}+\text{FN}) \quad (3)$$

$$F1-\text{score} = 2\times\text{Recall}\times\text{Precision}/(\text{Recall}+\text{Precision}). \quad (4)$$

Here, TP refers to the number of pixels in the pig farms that were correctly extracted, TN refers to the number of pixels without pig farms that were correctly extracted, FP denotes the number of nonpig farm pixels that were misclassified as buildings, and FN denotes the number of pig farm pixels that were not identified.

IV. Results

A. Extraction Accuracy With Different Combinations of GaoFen Satellite Data

The pig farms were identified with considerable accuracy in experiments A, C, and D, while the accuracy of experiment B was relatively lower (see Fig. 4). The average OA using GF-2, the combination of GF-2 and GF-7, the combination of GF-2 and GF-5, and GF-5 were 94.97%, 94.49%, 93.6%, and 88.37%, respectively (see Fig. 5).

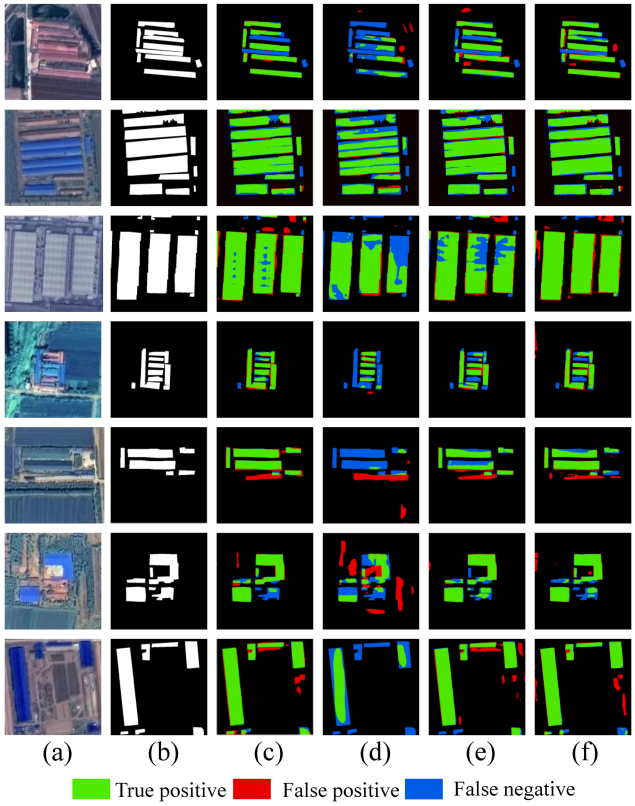

Fig. 4. Comparison of pig farm extraction results of four experimental groups. (a) GF-2 image. (b) Ground survey. (c) Group A. (d) Group B. (e) Group C. (f) Group D. Green indicates true positive (TP), red indicates false positive (FP), and blue indicates false negative (FN) results. TP denotes correctly classified pixels of pig farms. FP and FN denote incorrectly classified pixels of pig farms and incorrectly classified pixels of nonpig farms, respectively.

Generally, most pixels within the farms could be identified based on GF-2 multispectral images, especially the pixels located at the boundary of the farms, which could also be extracted. These features made the results look like regular patches even though there were still some pixels that were identified as non-pig farm pixels. More pig farm pixels were misidentified based on GF-5 hyperspectral satellite images. The results based on the combination of GF-2 and GF-5 were better than the results using only GF-5 data, but there was still some misidentification using that combination than with the use of only GF-2 data. The results based on the combination of GF-2 and GF-7 had clearer boundaries, more regular patches, and less salt-and-pepper noise caused by misidentification.

The pixels containing small-scale pig farms had a higher possibility of being undetected. The pixels containing large-scale farms could be extracted in more regular patches with evident boundaries, although a small proportion of them were not identified.

For each experimental group, the average OA for ten times was above 80%. The recall, OA and F1-score were consistent between these four groups (see Fig. 5). In general, identification was highly accurate using GF-2 multispectral images

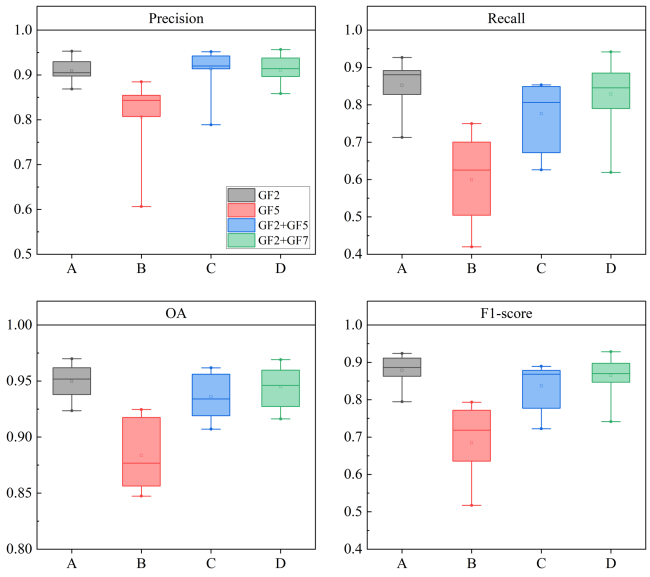

Fig. 5. Boxplots of precision, recall, OA, and F1-score in the tenfold cross validation for four experimental groups. The solid black lines indicate the medians.

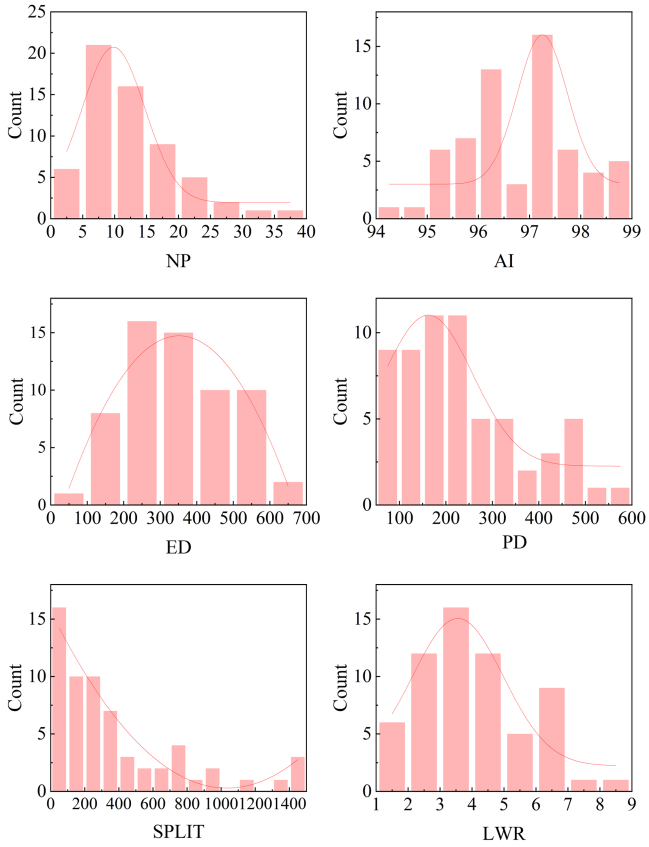

Fig. 6. Histogram of pig farm landscape pattern indices at the patch scale.

independently, with precision, recall, and overall accuracy values of 90.96%, 85.22%, and 94.97%, respectively. Compared with group A, the identifications in group C and group D were improved by 0.4% and 0.1%, respectively, with the increase in precision, with the ancillary support of hyperspectral images sourced from GF-5 and DSM sourced from GF-7. The results of using the combination of GF-2 and GF-5 achieved a higher average precision with a higher stability and a lower variance, even though the recall result showed a relatively lower average than did the use of the GF-2 and GF-7 combination. This indicated that the combination of GF-2 and GF-7 presented a slight advantage in identifying more farm pixels correctly. There was more omission error with a recall of 59.91% when identification was based on hyperspectral images from only GF-5.

B. Extraction Accuracy of Pig Farms With Different Morphological Characteristics

The pig farms examined in this study exhibited high levels of aggregation and density. To describe the morphological characteristics of the pig farms, six landscape pattern indices, number of patches (NP), aggregation index (AI), edge density (ED), splitting index (SPLIT), patch density (PD), and length-to-width ratio (LWR), were selected. Specifically, the NP of 70% of pig farms was less than 15, and the AI of all pig farms was between 94 and 99. Pig farms with an ED of greater than 200 and a PD of greater than 100 each accounted for more than 80% of all pig farms. The distribution of SPLIT was relatively scattered. For all pig farms, the average LWR of their patches was greater than 1, and for 70% of them, the ratios were greater than 3, indicating that the majority of the pig farms had an elongated rectangular shape (see Fig. 6).

Overall, deep learning had a higher accuracy in extracting pig farms with large NPs and a high AI, and a lower accuracy in extracting pig farms with high ED and PD values (see Fig. 7). The relationship between OA and morphological characteristics indicated that the NP and the AI showed a relatively obviously positive correlation with OA. The ED and PD were negatively correlated with OA. There was a slight difference in the identification accuracy of farms with different SPLIT and LWR.

V. Discussion

Four groups of experiments were designed to verify the effectiveness of GaoFen images for pig farm extraction. Among these experiments, the error was mainly caused by omission, while commission errors occasionally appeared. Some information was found by comparing the pig farm identification accuracies of different combinations of GF images.

1) The spatial detail information provided by high spatial resolution data play a more important role in improving the pig farm identification accuracy than did the spectral detail information provided by the hyperspectral data. Pig farm extraction based on high-resolution multispectral data could obtain identification results with the best precision. The recall, accuracy, and F1-score were higher and more stable using these data than those of the other three groups, with fewer false detections and missed detections.
2) Although the GF-5 hyperspectral data provided more spectral information of pig farms than did the GF-2 multispectral data, its lower spatial resolution constrained its

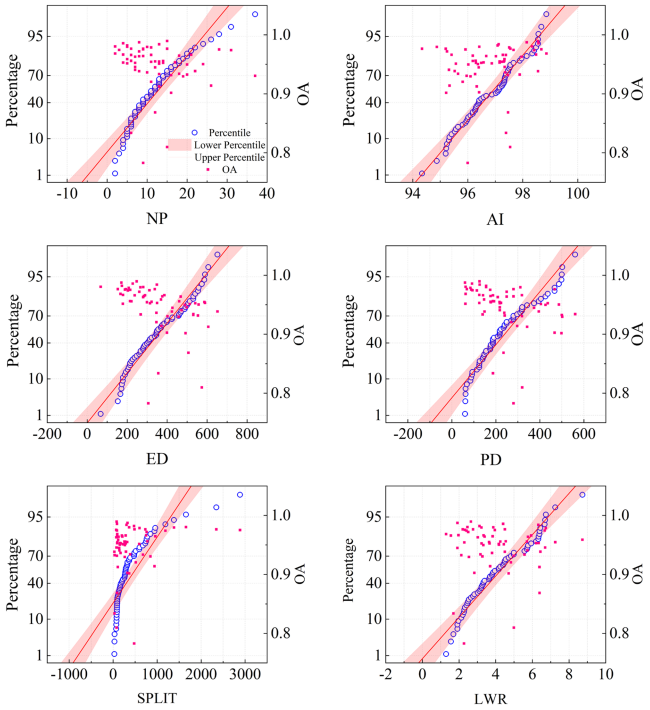

Fig. 7. Percentile plots of pig farm landscape pattern indices and scatter plots of the overall accuracy of pig farm extraction.

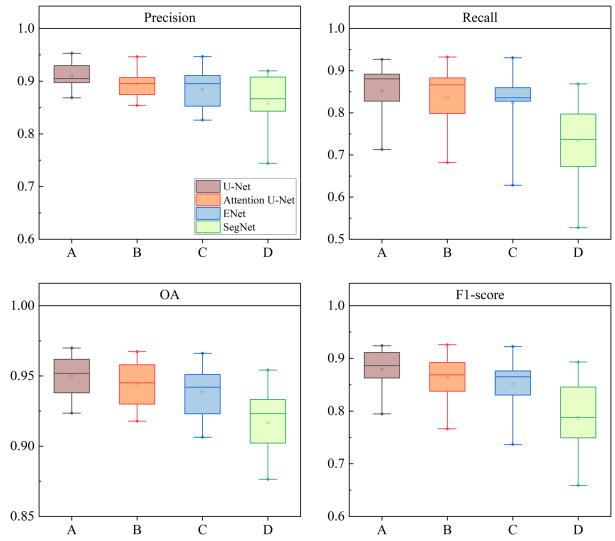

Fig. 8. Boxplots of precision, recall, OA, and F1-score in the tenfold cross validation for four deep learning models.

ability to identify small architectural structures. Because lower spatial resolution data resulted in the poor identification of small buildings, large areas of small buildings were missed. The four accuracy evaluation indicators performed the worst with GF-5 data.

3) The registration error caused by spatially different resolutions between GF-5 and GF-2 was the reason for the lower accuracy when using GF-5. The identification accuracy based on the combination of GF-2 multispectral data and GF-5 hyperspectral data was higher than that based on GF-5 data alone but lower than that based on GF-2 data alone.
4) The DSM derived from GF-7 helped improve pig farm identification by reducing omission errors. When the building roofs were obscured by shadows or decorated with other materials, this led to abnormal spectra on GF-2 data. Thus, combining GF-2 and GF-7 provides an effective solution to achieve better results, although the registration errors of GF-2 and GF-7 cannot be ignored.

In addition to the registration errors caused by the different data sources, the temporal differences between the different data sources can also introduce certain errors in pig farm identification using deep learning algorithms. Because different sensors have different revisit cycles, it is difficult to obtain data from different sources on the same dates at the same locations. Considering China's statistical surveys on pig farming are conducted once a year, efforts should still be made to ensure that a year is not skipped in the acquisition of data from different sources, even though pig farm buildings do not change much within a year in general. If the government issues temporary restrictions or bans on pig farming in a particular year due to urban planning, the time intervals between different data sources need to be more frequent. To evaluate the effectiveness of different deep learning networks on pig farm identification, Attention U-Net, Enet, and SegNet were applied to GF-2 dataset for pig farm identification [43], [44], [54]. Each experiment was repeated ten times, and the results were compared with those of U-Net (see Fig. 8). The comparison results on four evaluation metrics demonstrate the effectiveness of deep learning methods on pig farm identification. The average OA for ten times with Attention U-Net, Enet, and SegNet are all above 90% with 94.35%, 93.84%, and 91.57%, respectively, while that of U-Net is 94.97%. The results also revealed that the network architecture had impact on pig farm identification. The performance of U-Net was slightly better than the other networks with significantly faster computation speed. It may because our dataset is relatively small compared to traditional computer vision datasets, which may not fully reflect the differences between networks.

Although this study achieved considerable results in identifying pig farms based on deep learning, it still has some limitations. First, due to the scattered distribution of the pig farm samples, sample collection is difficult, and the number of training samples used in this study was less than that used for object recognition in the computer vision field [55], [56]. Because of the small sample size, tenfold cross validation was employed for accuracy evaluation. In addition, the limited number of samples made it difficult to fully cover various forms of pig farms and obtain sufficiently representative samples. In future studies, collecting more diverse samples from pig farms will improve the completeness and representativeness of the samples. Second, whether pig farms can be effectively distinguished from residential and industrial areas is a subject that requires further experimentation and exploration. In this study, there are no typically industrial facilities or residential buildings around pig farms, because the site selection for pig farms in China takes into consideration environmental concerns such as the disposal of pig excrement

and the spread of diseases. However, there are office buildings near pig farming facilities, which are labeled and recognized as nonfarms in this study. The results and accuracy evaluation reflects that the methods proposed in this study can effectively identify pig farms and other buildings. Third, although deep learning networks have been shown to have good transferability, the model in this study has not yet been applied to identify more regions and small-scale pig farms. Fourth, techniques in the field of machine learning, such as semisupervised [57], one-class classification [58], and few-shot [59] learning techniques, may be helpful to train the U-Net model with a small amount of labelled data and a large amount of unlabeled data, which can promote the generalization ability of the model.

Pig farms are generally composed of some elongated buildings, but the shape and distribution of the buildings can vary. For large-scale pig farms, buildings are generally relatively large and similar in appearance, with a large NP, high AI, and high extraction accuracy. Small pig farms have smaller buildings with inconsistent appearances. These pig farms generally have a higher ED and patch density (PD) and a lower extraction accuracy. To improve pig farm identification, future research should focus on small pig farms and develop identification methods that account for the architectural characteristics of these farms.

At present, deep learning methods are being applied in various fields related to pig farming, such as pig counting [60], pig posture detection [61], and pig behavior recognition [62]. This study focuses on the automatic extraction of spatial distribution information on pig farms, which enriches the research on deep learning in the field of pig farming and has significant implications for improving the management of pig farms and pork production estimates.

VI. Conclusion

Accurate information on the spatial distribution and area of pig farms is crucial for pig farming management, environmental governance, and disease prevention and control. However, the relevant governmental regulatory departments currently rely on field surveys, which are not very efficient, and few studies have focused on extracting spatial information on pig farms using remote sensing data. This study proposed a method to understand the spatial distribution of pig farms using the U-Net deep learning model. A series of experiments were conducted based on different GaoFen satellite image combinations to illustrate the applicability of multisource GaoFen satellite images for pig farm extraction and the impact of the morphological features of the farms on their identification accuracy. The results demonstrated that pig farms could be effectively identified by the U-Net model using different combinations of GaoFen data, with an average OA of over 80%. The high identification accuracy achieved using GF-2 multispectral imagery indicated that high spatial resolution data played an essential role in ensuring pig farm identification accuracy. Hyperspectral information from GF-5 and DSM information from GF-7 helped improve pig farm identification, with clearer boundaries, more regular patches, less salt and pepper noise, and fewer missed detections, but their lower spatial resolutions and registration errors may restrain their ability to identify small architectural structures. In addition, the deep learning algorithm showed a higher accuracy in extracting pig farms with a greater NP and a higher AI, and it presented a lower accuracy in identifying pig farms with a higher ED and higher PD. Although there are still some limitations to address, for example, by improving the deep learning networks model and enlarging the sample pool for various sizes of pig farms, this study enriches the research on the use of deep learning for pig farm identification and provides a scientific reference for governmental decision-making on pig breeding management.

References

[1] S. Shimokawa, "Sustainable meat consumption in China," *J. Integrative Agriculture*, vol. 14, no. 6, pp. 1023–1032, 2015, doi: 10.1016/s2095-3119(14)60986-2.

[2] Y. N. He, X. G. Yang, J. Xia, L. Y. Zhao, and Y. X. Yang, "Consumption of meat and dairy products in China: A review," *Proc. Nutr. Soc.*, vol. 75, no. 3, pp. 385–391, Aug. 2016, doi: 10.1017/s0029665116000641.

[3] X. T. Zhou et al., "Emergence of African swine fever in China, 2018," *Transboundary Emerg. Dis.*, vol. 65, no. 6, pp. 1482–1484, Dec. 2018, doi: 10.1111/tbed.12989.

[4] E. Mighell and M. P. Ward, "African swine fever spread across Asia, 2018–2019," *Transboundary Emerg. Dis.*, vol. 68, no. 5, pp. 2722–2732, Sep. 2021, doi: 10.1111/tbed.14039.

[5] X. H. Zhang et al., "Changing structure and sustainable development for China's hog sector," *Sustainability*, vol. 9, no. 1, pp. 69–83, Jan. 2017, doi: 10.3390/su9010069.

[6] M. X. Han, W. S. Yu, and F. Clora, "Boom and bust in China's pig sector during 2018-2021: Recent recovery from the ASF shocks and longer-term sustainability considerations," *Sustainability*, vol. 14, no. 11, Jun. 2022, Art. no. 6784, doi: 10.3390/su14116784.

[7] F. Zhang and F. Wang, "Prediction of pork supply via the calculation of pig population based on population prediction model," *Int. J. Agricultural Biol. Eng.*, vol. 13, no. 2, pp. 208–217, Mar. 2020, doi: 10.25165/j.ijabe.20201302.5303.

[8] G. Machado, J. A. Galvis, F. P. N. Lopes, J. Voges, A. A. R. Medeiros, and N. C. Cardenas, "Quantifying the dynamics of pig movements improves targeted disease surveillance and control plans," *Transboundary Emerg. Dis.*, vol. 68, no. 3, pp. 1663–1675, May 2021, doi: 10.1111/tbed.13841.

[9] M. Weiss, F. Jacob, and G. Duveiller, "Remote sensing for agricultural applications: A meta-review," *Remote Sens. Environ.*, vol. 236, Jan. 2020, Art. no. 111402, doi: 10.1016/j.rse.2019.111402.

[10] S. K. Lowder, J. Skoet, and T. Raney, "The number, size, and distribution of farms, smallholder farms, and family farms worldwide," *World Develop.*, vol. 87, pp. 16–29, Nov. 2016, doi: 10.1016/j.worlddev.2015.10.041.

[11] R. P. Sishodia, R. L. Ray, and S. K. Singh, "Applications of remote sensing in precision agriculture: A review," *Remote Sens.*, vol. 12, no. 19, Oct. 2020, Art. no. 3136, doi: 10.3390/rs12193136.

[12] N. Zang, Y. Cao, Y. Wang, B. Huang, L. Zhang, and P. T. Mathiopoulos, "Land-use mapping for high-spatial resolution remote sensing image via deep learning: A review," *IEEE J. Sel. Topics Appl. Earth Observ. Remote Sens.*, vol. 14, pp. 5372–5391, 2021, doi: 10.1109/jstars.2021.3078631.

[13] C. Zheng, Y. Liu, B. Bluemling, A. P. J. Mol, and J. Chen, "Environmental potentials of policy instruments to mitigate nutrient emissions in Chinese livestock production," *Sci. Total Environ.*, vol. 502, pp. 149–156, Jan. 2015, doi: 10.1016/j.scitotenv.2014.09.004.

[14] J. Li, X. Huang, L. Tu, T. Zhang, and L. Wang, "A review of building detection from very high resolution optical remote sensing images," *GIScience Remote Sens.*, vol. 59, no. 1, pp. 1199–1225, Dec. 2022, doi: 10.1080/15481603.2022.2101727.

[15] A. K. Shackelford and C. H. Davis, "A combined fuzzy pixel-based and object-based approach for classification of high-resolution multispectral data over urban areas," *IEEE Trans. Geosci. Remote Sens.*, vol. 41, no. 10, pp. 2354–2363, Oct. 2003, doi: 10.1109/tgrs.2003.815972.

[16] M. Pesaresi et al., "A global human settlement layer from optical HR/VHR RS data: Concept and first results," *IEEE J. Sel. Topics Appl. Earth Observ. Remote Sens.*, vol. 6, no. 5, pp. 2102–2131, Oct. 2013, doi: 10.1109/jstars.2013.2271445.

[17] M. K. Firozjaei, A. Sedighi, M. Kiavarz, S. Qureshi, D. Haase, and S. K. Alavipanah, "Automated built-up extraction index: A new technique for mapping surface built-up areas using LANDSAT 8 OLI imagery," *Remote Sens.*, vol. 11, no. 17, Sep. 2019, Art. no. 1966, doi: 10.3390/rs11171966.

[18] H. M. Rizeei, B. Pradhan, and M. A. Saharkhiz, "Urban object extraction using Dempster Shafer feature-based image analysis from worldview-3 satellite imagery," *Int. J. Remote Sens.*, vol. 40, no. 3, pp. 1092–1119, Feb. 2019, doi: 10.1080/01431161.2018.1524173.

[19] A. Varshney, "Improved NDBI differencing algorithm for built-up regions change detection from remote-sensing data: An automated approach," *Remote Sens. Lett.*, vol. 4, no. 5, pp. 504–512, May 2013, doi: 10.1080/2150704x.2013.763297.

[20] H. Xu, "A new index for delineating built-up land features in satellite imagery," *Int. J. Remote Sens.*, vol. 29, no. 14, pp. 4269–4276, 2008, doi: 10.1080/01431160802039957.

[21] X. Huang and L. Zhang, "Morphological building/shadow index for building extraction from high-resolution imagery over urban areas," *IEEE J. Sel. Topics Appl. Earth Observ. Remote Sens.*, vol. 5, no. 1, pp. 161–172, Feb. 2012, doi: 10.1109/jstars.2011.2168195.

[22] J. Abellan and S. Moral, "Building classification trees using the total uncertainty criterion," *Int. J. Intell. Syst.*, vol. 18, no. 12, pp. 1215–1225, Dec. 2003, doi: org/10.1002/int.10143.

[23] J. Niemeyer, F. Rottensteiner, and U. Soergel, "Contextual classification of lidar data and building object detection in urban areas," *ISPRS J. Photogrammetry Remote Sens.*, vol. 87, pp. 152–165, Jan. 2014, doi: 10.1016/j.isprsjprs.2013.11.001.

[24] X. Huang and L. P. Zhang, "An SVM ensemble approach combining spectral, structural, and semantic features for the classification of high-resolution remotely sensed imagery," *IEEE Trans. Geosci. Remote Sens.*, vol. 51, no. 1, pp. 257–272, Jan. 2013, doi: 10.1109/tgrs.2012.2202912.

[25] M. Turker and D. Koc-San, "Building extraction from high-resolution optical spaceborne images using the integration of support vector machine (SVM) classification, Hough transformation and perceptual grouping," *Int. J. Appl. Earth Observ. Geoinf.*, vol. 34, pp. 58–69, Feb. 2015, doi: 10.1016/j.jag.2014.06.016.

[26] X. X. Zhu et al., "Deep learning in remote sensing," *IEEE Geosci. Remote Sens. Mag.*, vol. 5, no. 4, pp. 8–36, Dec. 2017, doi: 10.1109/mgrs.2017.2762307.

[27] A. Kamilaris and F. X. Prenafeta-Boldu, "A review of the use of convolutional neural networks in agriculture," *J. Agricultural Sci.*, vol. 156, no. 3, pp. 312–322, Apr. 2018, doi: 10.1017/s0021859618000436.

[28] J. Y. Li, X. Huang, and J. Y. Gong, "Deep neural network for remote-sensing image interpretation: Status and perspectives," *Nat. Sci. Rev.*, vol. 6, no. 6, pp. 1082–1086, Nov. 2019, doi: 10.1093/nsr/nwz058.

[29] J. X. Gu et al., "Recent advances in convolutional neural networks," *Pattern Recognit.*, vol. 77, pp. 354–377, May 2018, doi: 10.1016/j.patcog.2017.10.013.

[30] A. Voulodimos, N. Doulamis, A. Doulamis, and E. Protopapadakis, "Deep learning for computer vision: A brief review," *Comput. Intell. Neurosci.*, vol. 2018, pp. 1–13, Feb. 2018, doi: 10.1155/2018/7068349.

[31] G. Cheng, X. Xie, J. Han, L. Guo, and G.-S. Xia, "Remote sensing image scene classification meets deep learning: Challenges, methods, benchmarks, and opportunities," *IEEE J. Sel. Topics Appl. Earth Observ. Remote Sens.*, vol. 13, pp. 3735–3756, 2020, doi: 10.1109/jstars.2020.3005403.

[32] K. M. He, X. Y. Zhang, S. Q. Ren, and J. Sun, "Delving deep into rectifiers: Surpassing human-level performance on imagenet classification," in *Proc. IEEE Int. Conf. Comput. Vis.*, 2015, pp. 1026–1034.

[33] J. Zhang, T. Fukuda, and N. Yabuki, "Development of a city-scale approach for façade color measurement with building functional classification using deep learning and street view images," *Int. Soc. Photogrammetry Remote Sens. Int. J. Geo-Inf.*, vol. 10, no. 8, p. 551–571, 2021.

[34] Y. Xu, Z. He, X. Xie, Z. Xie, J. Luo, and H. Xie, "Building function classification in Nanjing, China, using deep learning," *Trans. Geographic Inf. Syst.*, vol. 26, no. 5, pp. 2145–2165, 2022.

[35] Y. Ma, S. Liu, G. Xue, and D. Gong, "Soft sensor with deep learning for functional region detection in urban environments," *Sensors*, vol. 20, no. 12, pp. 33–48, 2020.

[36] Z. Bai, J. Zhao, Z. Wei, X. Jin, and L. Ma, "Socio-economic drivers of pig production and their effects on achieving sustainable development goals in China," *J. Integrative Environ. Sci.*, vol. 16, no. 1, pp. 141–155, 2019.

[37] H. Van de Weerd and S. Ison, "Providing effective environmental enrichment to pigs: How far have we come?," *Animals*, vol. 9, no. 5, p. 254–275, 2019.

[38] S. Shrestha and L. Vanneschi, "Improved fully convolutional network with conditional random fields for building extraction," *Remote Sens.*, vol. 10, no. 7, Jul. 2018, Art. no. 1135, doi: 10.3390/rs10071135.

[39] E. Maltezos, N. Doulamis, A. Doulamis, and C. Ioannidis, "Deep convolutional neural networks for building extraction from orthoimages and dense image matching point clouds," *J. Appl. Remote Sens.*, vol. 11, pp. 042620–042620, Dec. 2017, doi: 10.1117/1.Jrs.11.042620.

[40] K. Men et al., "Deep deconvolutional neural network for target segmentation of nasopharyngeal cancer in planning computed tomography images," *Front. Oncol.*, vol. 7, p. 315–323, Dec. 2017, doi: 10.3389/fonc.2017.00315.

[41] C. Zhang et al., "An object-based convolutional neural network (OCNN) for urban land use classification," *Remote Sens. Environ.*, vol. 216, pp. 57–70, Oct. 2018, doi: 10.1016/j.rse.2018.06.034.

[42] O. Ronneberger, P. Fischer, and T. Brox, "U-net: Convolutional networks for biomedical image segmentation," in *Medical Image Computing and Computer-Assisted Intervention – MICCAI 2015* (Lecture Notes in Computer Science). Cham, Switzerland: Springer, 2015, pp. 234–241.

[43] A. Paszke, A. Chaurasia, S. Kim, and E. J. Culurciello, "Enet: A deep neural network architecture for real-time semantic segmentation," p. 10, Jun. 2016, *arXiv: 1606.02147*.

[44] V. Badrinarayanan, A. Kendall, and R. Cipolla, "SegNet: A deep convolutional encoder-decoder architecture for image segmentation," *IEEE Trans. Pattern Anal. Mach. Intell.*, vol. 39, no. 12, pp. 2481–2495, Dec. 2017, doi: 10.1109/tpami.2016.2644615.

[45] Z. Zhang, Q. Liu, and Y. Wang, "Road extraction by deep residual U-Net," *IEEE Geosci. Remote Sens. Lett.*, vol. 15, no. 5, pp. 749–753, May 2018, doi: 10.1109/lgrs.2018.2802944.

[46] Z. Q. Liu, Y. W. Cao, Y. Z. Wang, and W. Wang, "Computer vision-based concrete crack detection using U-net fully convolutional networks," *Automat. Construction*, vol. 104, pp. 129–139, Aug. 2019, doi: 10.1016/j.autcon.2019.04.005.

[47] N. Ibtehaz and M. S. Rahman, "MultiResUNet : Rethinking the U-Net architecture for multimodal biomedical image segmentation," *Neural Netw.*, vol. 121, pp. 74–87, Jan. 2020, doi: 10.1016/j.neunet.2019.08.025.

[48] Y. Zheng, Q. Shen, M. Wang, M. Yang, J. Huang, and C. Feng, "Semantic segmentation sample augmentation based on simulated scene generation-case study on dock extraction from high spatial resolution imagery," *Int. J. Remote Sens.*, vol. 42, no. 13, pp. 4961–4984, 2021.

[49] F. Liu and L. Wang, "UNet-based model for crack detection integrating visual explanations," *Construction Building Mater.*, vol. 322, pp. 126–265, 2022.

[50] B. J. Yan, J. J. Yan, W. J. Shi, and Y. X. Li, "Study on the comprehensive comparative advantages of pig production and development in China based on geographic information system," *Clean Technol. Environ. Policy*, vol. 22, no. 1, pp. 105–117, Jan. 2020, doi: 10.1007/s10098-019-01772-3.

[51] D. Li, M. Wang, and J. Jiang, "China's high-resolution optical remote sensing satellites and their mapping applications," *Geo-Spatial Inf. Sci.*, vol. 24, no. 1, pp. 85–94, Jan. 2021, doi: 10.1080/10095020.2020.1838957.

[52] Y.-N. Liu et al., "The advanced hyperspectral imager aboard China's GaoFen-5 satellite," *IEEE Geosci. Remote Sens. Mag.*, vol. 7, no. 4, pp. 23–32, Dec. 2019, doi: 10.1109/mgrs.2019.2927687.

[53] Y. Sun et al., "GF-5 satellite: Overview and application prospects," *Spacecraft Recovery Remote Sens.*, vol. 39, no. 3, pp. 1–13, 2018.

[54] O. Oktay et al., "Attention U-net: Learning where to look for the pancreas," Apr. 2018, *arXiv:1804.03999*.

[55] I. Demir et al., "DeepGlobe 2018: A challenge to parse the earth through satellite images," in *Proc. IEEE Comput. Soc. Conf. Comput. Vis. Pattern Recognit. Workshops*, 2018, pp. 172–181.

[56] S. Ji, S. Wei, and M. Lu, "Fully convolutional networks for multisource building extraction from an open aerial and satellite imagery data set," *IEEE Trans. Geosci. Remote Sens.*, vol. 57, no. 1, pp. 574–586, Jan. 2019, doi: 10.1109/tgrs.2018.2858817.

[57] D. H. Lee, "Pseudo-label: The simple and efficient semi-supervised learning method for deep neural networks," in *Proc. Int. Conf. Mach. Learn. Workshop: Challenges Representation Learn.*, 2013, pp. 1–6.

[58] J. Munoz-Mari, F. Bovolo, L. Gomez-Chova, L. Bruzzone, and G. Camps-Valls, "Semisupervised one-class support vector machines for classification of remote sensing data," *IEEE Trans. Geosci. Remote Sens.*, vol. 48, no. 8, pp. 3188–3197, Aug. 2010, doi: 10.1109/tgrs.2010.2045764.

[59] Y. Wang, Q. Yao, J. T. Kwok, and L. M. Ni, "Generalizing from a few examples: A survey on few-shot learning," *Assoc. Comput. Machinery Comput. Surv.*, vol. 53, no. 3, pp. 1–34, Jun. 2020, doi: 10.1145/3386252.

[60] M. X. Tian, H. Guo, H. Chen, Q. Wang, C. J. Long, and Y. H. Ma, "Automated pig counting using deep learning," *Comput. Electron. Agriculture*, vol. 163, Aug. 2019, Art. no. 104840, doi: 10.1016/j.compag.2019.05.049.

[61] M. Riekert, A. Klein, F. Adrion, C. Hoffmann, and E. Gallmann, "Automatically detecting pig position and posture by 2D camera imaging and deep learning," *Comput. Electron. Agriculture*, vol. 174, Jul. 2020, Art. no. 105391, doi: 10.1016/j.compag.2020.105391.

[62] A. Alameer, I. Kyriazakis, H. A. Dalton, A. L. Miller, and J. Bacardit, "Automatic recognition of feeding and foraging behaviour in pigs using deep learning," *Biosyst. Eng.*, vol. 197, pp. 91–104, Sep. 2020, doi: 10.1016/j.biosystemseng.2020.06.013.

Jielin Guan received the master's degree in public administration from the School of Management, Guangdong University of Technology, Guangzhou, China, in 2023.

Her research interests include remote sensing application in agriculture and deep learning in remote sensing images.

Le Li received the B.S. degree in sciences and techniques of remote sensing from Wuhan University, Wuhan, China, in 2007, and the Ph.D. degree in cartography and geographic information system from Beijing Normal University, Beijing, China, in 2012.

She is currently an Associate Professor with the School of Management, Guangdong University of Technology, Guangzhou, China. Her research interests include remote sensing application in agriculture and land resource management, including deep learning in remote sensing images.

Zurui Ao received the M.S. and Ph.D. degrees in cartography and geographical information systems from Capital Normal University, Beijing, China, in 2014 and 2018, respectively.

He was a Postdoctoral Researcher with Sun Yat-sen University, Guangzhou, China, from 2018 to 2021. He is currently an Associate Researcher with the Beidou Research Institute, Faculty of Engineering, South China Normal University, Guangzhou. His research interests include light detection and ranging (LiDAR), deep learning in remote sensing images, and spatiotemporal fusion.

Kefei Zhao received the B.S. degree in geography information system from Henan University, Kaifeng, China, in 2011, the M.S. degree in cartography and geography information system from Sun Yat-sen University, Guangzhou, China, in 2013, and the Ph.D. degree in cartography and geography information system from Sun Yat-sen University, Guangzhou, China, in 2017.

He is currently a Lecturer with School of Management, Guangdong University of Technology, Guangzhou, China. His research interests include application of remote sensing and land use modeling.

Yaozhong Pan received the M.S. and the Ph.D. degrees in physical geography from Beijing Normal University, Beijing, China, in 1994 and 1997, respectively.

He is currently a Professor with Beijing Normal University. His main research interests include deep learning in remote sensing images, including remote sensing applications in agriculture statistics and disaster risk assessment.

Weifeng Ma received the Ph.D. degree in cartography and geographic information system from the School of Resources, Beijing Normal University, Beijing, China, in 2011.

He is currently the Director of Smart Agriculture Division, PIESAT Information Technology Company, Ltd., Beijing. His main research interests include agricultural remote sensing, including remote sensing monitoring of agricultural resources and agricultural production process.